Properties of the Nucleo-Olivary Pathway: An *In Vivo* Whole-Cell Patch Clamp Study

Paolo Bazzigaluppi[1]**, Tom Ruigrok**[1]**, Payam Saisan**[2]**, Chris I. De Zeeuw**[1,3]**, Marcel de Jeu**[1]*

1 Department of Neuroscience, Erasmus Medical Center Rotterdam, Rotterdam, The Netherlands, **2** Department of Neuroscience, University of California San Diego, La Jolla, California, United States of America, **3** Netherlands Institute for Neuroscience, Amsterdam, The Netherlands

Abstract

The inferior olivary nucleus (IO) forms the gateway to the cerebellar cortex and receives feedback information from the cerebellar nuclei (CN), thereby occupying a central position in the olivo-cerebellar loop. Here, we investigated the feedback input from the CN to the IO *in vivo* in mice using the whole-cell patch-clamp technique. This approach allows us to study how the CN-feedback input is integrated with the activity of olivary neurons, while the olivo-cerebellar system and its connections are intact. Our results show how IO neurons respond to CN stimulation sequentially with: *i)* a short depolarization (EPSP), *ii)* a hyperpolarization (IPSP) and *iii)* a rebound depolarization. The latter two phenomena can also be evoked without the EPSPs. The IPSP is sensitive to a $GABA_A$ receptor blocker. The IPSP suppresses suprathreshold and subthreshold activity and is generated mainly by activation of the $GABA_A$ receptors. The rebound depolarization re-initiates and temporarily phase locks the subthreshold oscillations. Lack of electrotonical coupling does not affect the IPSP of individual olivary neurons, nor the sensitivity of its $GABA_A$ receptors to blockers. The GABAergic feedback input from the CN does not only temporarily block the transmission of signals through the IO, it also isolates neurons from the network by shunting the junction current and re-initiates the temporal pattern after a fixed time point. These data suggest that the IO not only functions as a cerebellar controlled gating device, but also operates as a pattern generator for controlling motor timing and/or learning.

Competing Interests: The authors have declared that no competing interests exist.

* E-mail: m.dejeu@erasmusmc.nl

Introduction

The inferior olive (IO) is located in the ventral medulla and gives rise to the climbing fibres (CFs), which constitute one of the two main excitatory inputs to the Purkinje cells (PCs) in the cerebellar cortex. Olivary neurons, which are coupled via dendro-dendritic gap junction (GJ) [1], also send off collaterals to the cerebellar nuclei (CN). PCs send inhibitory fibres to the CN, which contain GABAergic, glycinergic and glutamatergic neurons. Part of the CN neurons projects directly to the IO via an inhibitory, GABAergic, pathway [2–6]; whereas another population of CN neurons excites the IO indirectly via nuclei located at the mesodiencephalic junction (MDJ) [7,8]. This olivo-cortico-nuclear projection (Figure 1A) forms the basis of the modular organization of the cerebellum [9]. Despite our anatomical knowledge on this nucleo-olivary projection, its role in motor control and motor learning is still under debate [10,11]. The GABAergic feedback inhibition on the IO might serve to gate motor learning in the cerebellar cortex [2,12] or to control the participation of IO neurons in a motor task by controlling the electrical coupling between olivary neurons [13–15].

Although the anatomical evidence of GABAergic inputs being present in the IO is overwhelming [3,7,16], electrophysiological experiments, surprisingly, failed to reveal the presence of spontaneous inhibitory potentials (IPSPs) when olivary neurons' activity was recorded *in vitro* [14,17–20] or *in vivo* [21–23]. The

only two *in vitro* studies in which olivary GABAergic IPSPs were observed [24,25], were performed under experimental conditions specifically designed to solely observe the GABAergic response. Both studies are important because they directly show the actual presence and the activation of $GABA_A$ receptors on the membrane of IO neurons. Devor et al. [25] showed additionally that there is a differential distribution of $GABA_A$ receptor subtypes between the dendrites and soma of IO neurons and Best and Regehr [24] showed that the release of GABA is exclusively asynchronous and that the synaptic transmission was extremely frequency dependent, which are all important properties in order to understand the GABAergic transmission in the IO. However, both studies did not explore the contribution of this inhibitory feedback action under physiological conditions.

For these reasons, we directly activated the CN with a stimulation electrode while performing whole-cell recording from the IO *in vivo*. Our approach succeeded in evoking inhibitory responses (IPSPs) in olivary neurons and allowed us to explore their relation with the subthreshold oscillatory behaviour of the neurons. Moreover, we pharmacologically block the $GABA_A$ receptors in the recorded neuron, showing the direct involvement of $GABA_A$ receptors, in line with Devor et al. [25]. Ultimately, we replicated the experiments in Connexin36 knock out animals to demonstrate that the evoked GABAergic IPSPs were generated on
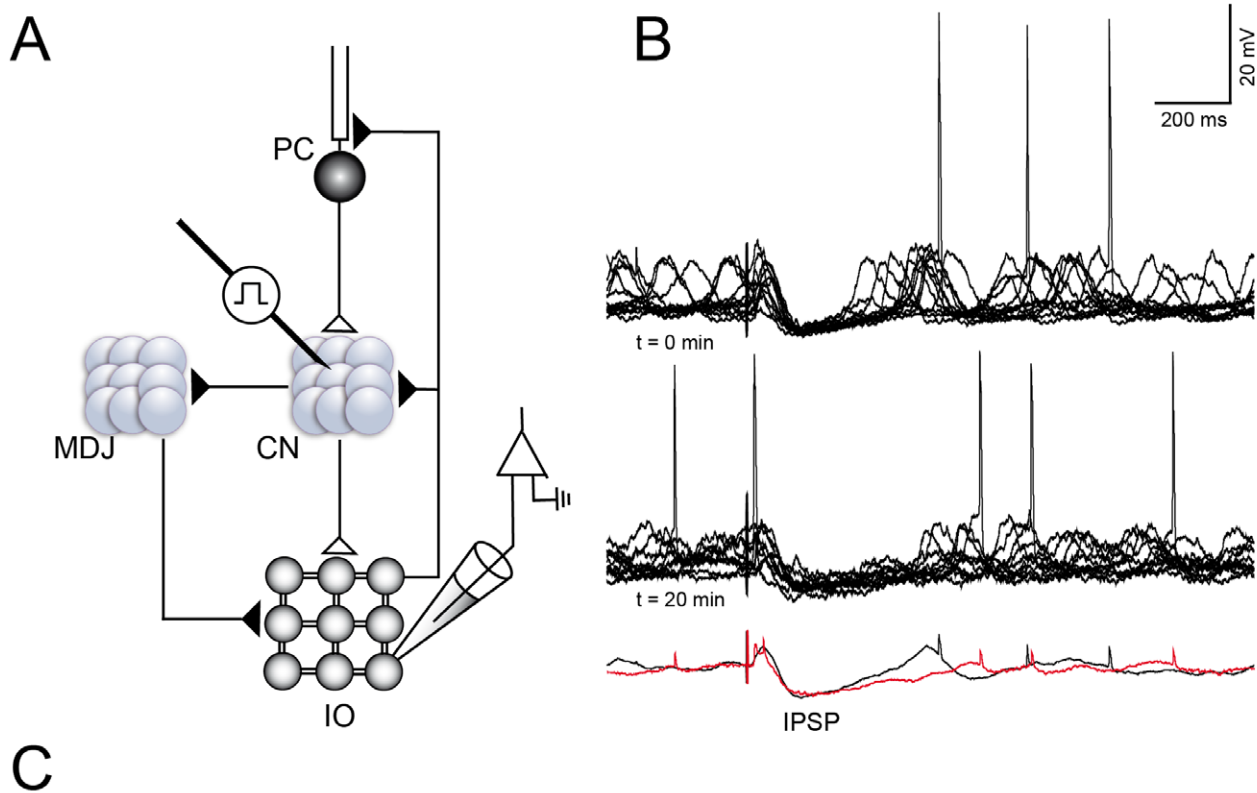
Figure 1. *In vivo* **CN-evoked IO response.** A: experimental set-up: the stimulation electrode is placed in CN, the recording pipette is in the IO. Synapse, closed triangle: excitatory, open triangle: inhibitory. B: control experiment, example of LTO cell responding to CN stimulation, top trace: beginning of the experiment (t = 0); middle trace: after twenty minutes (t = 20), bottom trace: averages of the two conditions above, black trace is t = 0; red trace is t = 20. There are no significant changes. C: coronal sections of cerebellum. Left: 1.6 magnifications, arrow points at the lesion in the Interpositus Nucleus, scale bar: 0.5 mm. Right: same as left, 4.6 magnifications, arrow points at the lesion, scale bar: 0.15 mm. Abbreviations: CN, Cerebellar Nuclei; MDJ, Meso-diencephalic Junction; PC, Purkinje Cell; IO, Inferior Olive.
doi:10.1371/journal.pone.0046360.g001

the recorded neuron and not in the periphery of the electrotonically coupled network.

Results

Cerebellar Control of the Inferior Olive

In vivo whole-cell recordings allow us to monitor both intrinsic suprathreshold and subthreshold activities of olivary neurons as well as responses evoked by CN stimulation (Figure 1). The recorded neurons presented subthreshold profiles in line with the ones previously shown by Khosrovani [22]. Briefly, we focused our analysis on the IO neurons which were presenting either low-threshold oscillations (LTO) or sinusoidal subthreshold oscillations (SSTO). It is still unknown whether these two different subthreshold activities reflect two distinct neuronal populations or whether they are two different oscillating profiles of the same type

of neurons. *The sinusoidal subthreshold oscillation is an intrinsic property [26–28], generate by a cascade of alternating channel activation [17] that includes the T-type Ca²⁺ channel Ca$_V$3.1.* What emerged from our study is that both LTO and SSTO neurons responded to CN stimulation, but in a different manner. For all the neurons that were orthodromically activated, we measured the passive membrane properties, which were similar to the ones reported by Khosrovani et al. [22]: the resting membrane potential of LTO cells was −53.5±6.2 mV (n = 20), whereas SSTO neurons showed a membrane potential of −54.0±6.2 mV (n = 15). Input resistance was on average 31.3±13.7 MΩ for LTO neurons and 23.5±4.9 MΩ for SSTO, whereas membrane capacitance was 202.5±108.5 pF and 236.6±89.7 pF for LTO and SSTO neurons respectively (see Table 1). The differences between LTO and SSTO neurons with regards to their subthreshold profile are limited to the frequency, the rhythm and the shape of the oscillations as already described by Khosrovani et al. [22]. The orthodromic activation of nucleo-olivary pathway by high-frequency stimulation of the CN gave rise to different sets of inhibitory responses. The activation of the nucleo-olivary pathway resulted in a very specific olivary response pattern (Figure 1B). Both LTO and SSTO neurons are able to respond to the CN stimulation with EPSPs after a latency of 38.15 (±14.2 ms, from here on, short-latency EPSPs), although with different probability (43.1% vs. 29.1% for LTO (n = 13) and SSTO (n = 7) neurons, respectively. Table 1). The EPSP, when present, was occasionally accommodating an action potential. The long-latency IPSPs responses were consistently recorded in both LTO (n = 13) and SSTO (n = 7) neurons (88.7% and 91.5% of the cases respectively) (Table 1). The long-latency IPSP fully suppressed the generation of action potentials as well as the generation of subthreshold activity, including oscillations; however, the responses of LTO and SSTO neurons express different characteristic in this respect. The duration of the membrane hyperpolarization in LTO neurons (573±292 ms, n = 13) was significantly longer than that observed in SSTO neurons (260±58 ms, n = 7; p<0.01, t-test, Table 1, Figure 2). Moreover, the IPSPs' peak amplitude of SSTO neurons was significantly bigger than the one of LTO neurons (−10.1±2.8 vs −6.6±1.4, p<0.01, t-test, Table 1). The long-latency IPSP responses (figure 2A and 2B) were observed with and without the preceding short-latency EPSPs, suggesting that these two responses are evoked independently from each other. We then stimulated two times in a row at different time intervals in four neurons that responded to CN stimulation with both a short-latency EPSPs and a long-latency IPSP in order to elucidate for how long the IPSP can prevent the onset of the EPSP evoked by the second stimulation. The second CN stimulation can elicit a second EPSP only if the interstimulus interval is at least 350 ms (n = 4, Fig. S1).

GABAergic Inhibitions and Subthreshold Oscillations

The most likely candidates responsible for the hyperpolarization are the GABA$_A$ receptors activated by the GABAergic pathway originating in the CN. In order to investigate the contribution of GABA in the observed long-latency hyperpolarizing responses, we added a specific GABA$_A$ receptor blocker DNDS to our pipette solution [29,30]. In order to block GABA$_A$ receptors internally, DNDS molecules have to travel from the pipette to distal dendritic sites; a time consuming process of approximately 20 minutes [30]. Therefore, this experiment requires a stable recording for at least 20 minutes. A subset of the neurons presented in Table 1 was recorded long enough to explore the properties of their responses over a time span of more than 20 minutes. To quantify the hyperpolarizing

response, we measured the duration, peak amplitude and surface area generated by the hyperpolarizing sag, which were not affected by the dialysis of the cytoplasm with our pipette solution (Table 2, Figure 1B). Control cells (n = 9) recorded for 20 minutes with a DNDS-free internal solution showed no significant difference in short-latency EPSPs probability, long-latency IPSPs probability, IPSPs duration, IPSP peak amplitude, IPSP area, rebound probability and amplitude between the beginning and the end of the recordings (Table 2). On the other hand, the presence of DNDS (n = 11) in the recording pipettes already affected some of the response properties that were measured immediately after breaking the membrane patch compared to the ones of control cells. The average probability, duration, surface area and peak amplitude of the IPSPs were lower, but not significantly, than the ones measured with DNDS-free solution, suggesting an immediate action of the blocker on somatic GABA$_A$ receptors (unpaired t-test, for SSTO, p = 0.06, p = 0.22, p = 0.84 and p = 0.42 respectively and for LTO, p = 0.14, p = 0.17, p = 0.19 and p = 0.29 respectively, Table 2). After 20 minutes of DNDS dialysis, the chances of triggering a hyperpolarizing response was significantly reduced (LTO: 85.3 vs 25.4, n = 7, p<0.01; SSTO: 93.5 vs 39.9, n = 4, p<0.01) and so was the peak amplitude (in mV, LTO: −6.5±1.5 vs −3.4±1, n = 7, p<0.01; SSTO: −10.96±3.9 vs −4.2±1.8, n = 4, p<0.01) and the surface area of the hyperpolarization (in ms*mV, LTO: 1737±599 vs 654±150, n = 7, p<0.01; SSTO: 1718±882 vs 484±254, n = 4, p = 0.04). On the other hand the chance of triggering the short latency EPSP was not significantly altered (Table 2) and, the chance to evoke a rebound depolarization were slightly but significantly reduced only in the case of SSTO neurons (96.5 vs 74.2, n = 4, p<0.05). Yet, the CN stimulations can still evoke a small hyperpolarizing response after 20 minutes of DNDS dialysis, (Figure 3, Table 2). In order to exclude the putative limiting blocking effects of 5 mM DNDS, two experiments have been performed with an high DNDS concentration (15 mM), but also the higher concentration of blocker was not able to fully remove the residual hyperpolarizing response (n = 2, Fig. S2). In fact, there was no difference between the effects following 15 mM and 5 mM DNDS, the latter concentration was then assumed to be sufficient to exert a maximal effect. The residual slow hyperpolarizing component is probably due to the activation of GABA$_B$ receptors which are present in the IO [31,32]. Unfortunately, there's no specific intracellular blocker for GABA$_B$ receptors, hence it was not possible in our experimental set up to investigate the role of this metabotropic GABAergic receptor.

Olivary neurons are electrotonically coupled through dendro-dendritic Connexin36 based gap junctions. Since GABA mediated currents can be transmitted from one cell to another via these gap junctions which are also structurally related to GABAergic synapses in olivary glomeruli [16,33], we aimed to show the importance of the electrical synapses in the expression of the CN evoked GABAergic transmission. Therefore, we replicated our experiments in mice that lack Connexin36 [23,26,27]. This experiment revealed that olivary responses to CN stimulation in Connexin36 knock-out mice were similar compared to those in wild type mice in that the hyperpolarizing response was also blocked by DNDS (Figure 3, Table 3). This result indicates that the olivary expression of the CN-evoked GABAergic synaptic transmission does not depend on the presence of an electrotonic network, consequently the responses we observed were generated by the activation of GABAreceptors on the primary (i.e. recorded) olivary cell and do not have a second or higher distant origin.
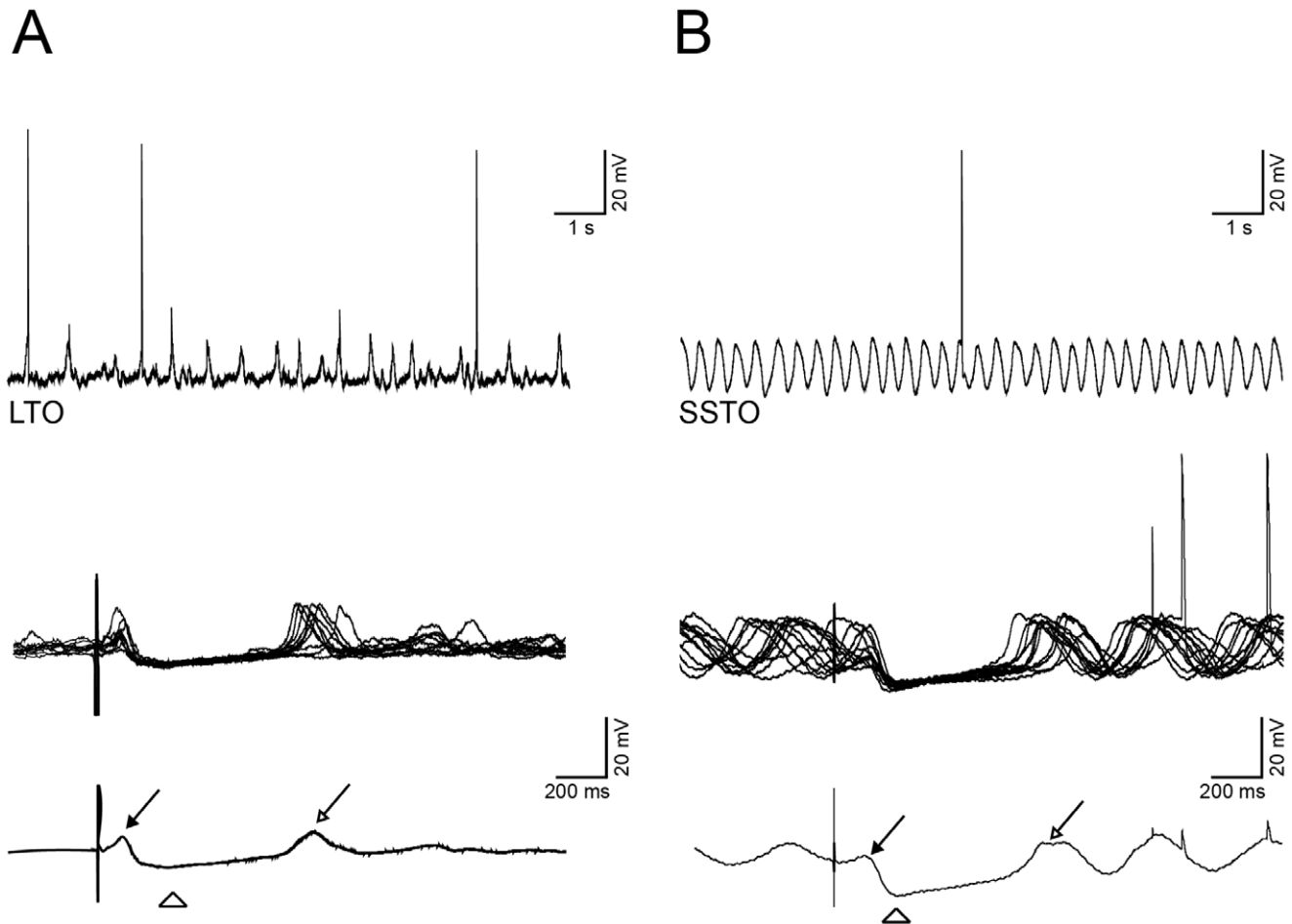
Figure 2. Differences in the response between LTO and SSTO neurons. A: spontaneous activity of an LTO cell (top left trace), then (middle trace) the same cell is responding to CN stimulation, bottom trace shows the average of the responses. B: same experiment but in a SSTO cell. Filled arrow: short-latency EPSP, empty arrow: rebound depolarization; empty arrowhead: peak of the IPSP.
doi:10.1371/journal.pone.0046360.g002

CN Stimulation Resets Subthreshold Oscillation

The long-latency IPSPs are terminated by a rebound depolarization (Figure 2, open arrow). The rebound depolarization is

Table 1. Passive properties and sub- and supra-threshold responses to CN stimulation of LTO and SSTO olivary neurons.

	LTO	SSTO
	Mean ± SD (n)	Mean ± SD (n)
Resting membrane potential (mV)	−53.5±6.2 (20)	−54.0±6.2 (15)
Input resistance (MΩ)	31.3±13.7 (20)	23.5±4.9 (15)
Membrane capacitance (pF)	202.5±108.5 (20)	236.6±89.7 (15)
Short latency EPSP (%)	43.1 (13) ±9.2	29.1 (7) ±5.6
Long latency IPSP (%)	88.7 (13) ±5.6	91.5 (7) ±4.6
IPSP duration (ms)	573±292 (13)*	260±58 (7)*
IPSP peak amplitude (mV)	−6.6±1.4 (13)*	−10.1±2.8 (7)*

*indicates significant difference.
doi:10.1371/journal.pone.0046360.t001

related to the evoked IPSP and requires also the activation of T-type Ca^{2+} channel $Ca_V3.1$ [34–36]. In SSTO neurons, the sinusoidal subthreshold oscillation resets after this rebound depolarization (Figure 2B and 3A). Given the fact that oscillations of LTO neurons are more arrhythmic and lack a proper phase, the reset was limited to the first oscillating bump. The resetting effect after the rebound depolarization is particularly evident when multiple traces are overlaid and averaged (Figure 2B and 3A, black lines, bottom traces). Before the stimulus artifact, the subthreshold oscillations (due to phase-indepent nature of the stimulus trigger) are out of phase and the average is, therefore, deprived of oscillatory behavior. However, after the rebound depolarization the subthreshold oscillations of multiple traces are locked in phase, resulting in a prominent sinusoidal wave when averaged (Figure 2B). With a pronounced release of GABA, the IO neuron will be isolated from the network for a longer period, and this can be measured as the time needed for the phase-lock to fade away. In order to measure the reset accuracy and the decay of the phase-lock, we performed cross-correlations between all the possible combinations of pairs of traces of the same cell (a total of 36 traces) using a running window approach (see materials and methods). All analyzed cells showed the highest phase-match during the IPSPs (i.e. when the effect of GABA is maximal), followed by the rebound depolarization (namely the first peak of the subthreshold
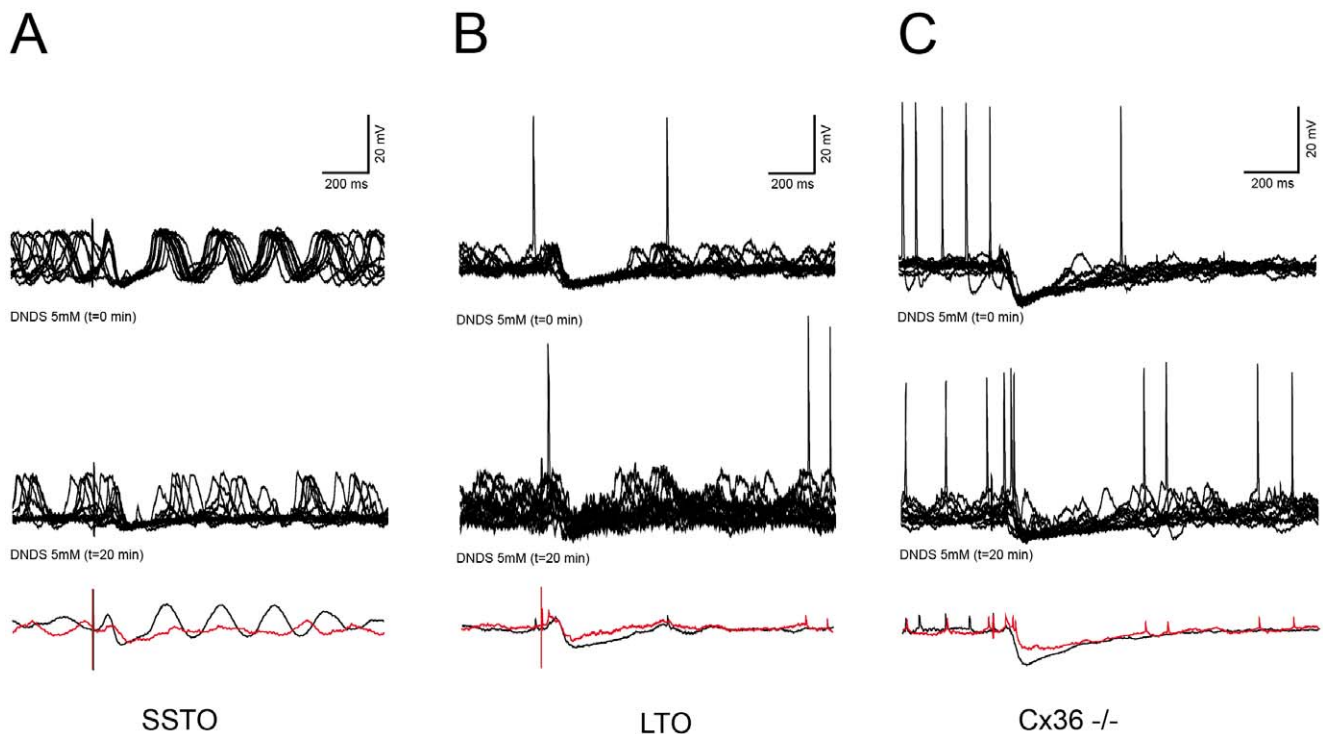
Figure 3. DNDS sensitivity in WT and Cx36 KO neurons. A: Wild type SSTO cell (top trace) responding to CN stimulation, then (middle trace) the response of the same cell to CN stimulation in reduced after 20 minutes of dialysis with DNDS, bottom trace represents the averages at the beginning of the experiment (black) and after 20 minutes of DNDS (red). B: same as A, but in a LTO cell. C: Cx36−/− LTO cell, the response and the DNDS sensitivity are not different from the Wild type.
doi:10.1371/journal.pone.0046360.g003

oscillation). Hereafter, the phase-match of the oscillation begins to deteriorate until the normalized cross-correlation value almost reaches zero. Figure 4A represents an example cell. The protocol was repeated 36 times in order to stimulate the cell at different random phase-points of its SSTO. All the traces from the same cell are overlaid in figure 4A (top). When the stimulation is given (red arrowhead) the neuron always responds with an IPSP, regardless the phase of the oscillation. A new oscillation is then initiated and its phase is reset in every repetition. The oscillation's phase induced by the IPSP drifts with time and after two cycles of oscillation it is shifted. The correlation index between all the combinations of pairs of repetitions is averaged and shown in figure 4A (bottom). Then, we wanted to measure the decay time of the phase-lock, because this would reflect the duration of the action of the GABAergic activation. Therefore we fitted the correlation indexes with a single exponential function (figure 4B, red line) and we extracted the decay constant for each recorded neuron. We then plotted the durations of the IPSP vs the decay constants of the phase-match deterioration process of all the neurons (Figure 4B, exponential fit: $r^2 = 0.83$, $n = 11$). We conclude that a longer inhibition comes together with a longer phase-lock in the oscillations and that both these phenomena possibly depend upon the amount of GABA released. Unfortunately, we could not explore this relationship in the presence of the GABA$_A$R blocker, because SSTO cells often lose their oscillation profile before the DNDS exerts its complete effect.

Overall, a short burst of stimulation of the nucleo-olivary pathway induces a prominent long-latency inhibition in olivary neurons. The IPSP resets the sinusoidal oscillations via the post inhibitory rebound depolarization and determines the phase of the following SSTOs.

Discussion

Cerebellar Control of the Inferior Olive

Due to the anatomical position of the IO, which is difficult to approach, its network properties have mainly been investigated by indirect measurements such as complex spikes activity in the cerebellar cortex [2,12,37,38] or by *in vitro* experiments [20,25]. Our work shows for the first time, *in vivo*, CN-evoked IPSPs in olivary neurons and their dependency on the activation of local GABA$_A$ receptors. Anatomical observations [3,38–41] have demonstrated the presence of inhibitory projections from the CN to the IO, and Devor et al. [25] showed that GABA$_A$ receptors can be activated on the soma and dendrites of IO neurons by puffing the GABA on different parts of the recorded neuron. The study of Best and Regehr [24] revealed that the release of GABA at CN to IO synapse is asynchronous. However, their olivary IPSPs/IPSCs were evoked *in vitro* via peri-olivary stimulation and by using an internal solution with high chloride concentration (to obtain a chloride reversal potential of −20 mV or 0 mV which amplifies the GABA$_A$ mediated response). In contrast, our experimental approach combines the time resolution of the whole-cell recordings with the advantages of having an *in vivo* preparation, where the network and the synaptic connections are intact [7]. The stimulation protocol that we used was set coherently with the high-frequency input that CN neurons receive from PC and that was shown to elicit a rebound depolarization with increased firing frequency in CN neurons [42]. This increased firing activity in the CN has been shown to play a prominent role in processing and storage of information regarding motor coordination such as the conditioning response in classical conditioning [43–46]. The connections between the

Table 2. Sub- and supra-threshold responses in Control and with presence of GABA$_A$ receptors blocker (DNDS).

	Oscill. behavior	Control				GABA$_A$ blocker DNDS			
		Immediately after break-in	>20 minutes after break in	p-value	n	Immediately after break-in	>20 minutes after break in	p-value	n
Short latency EPSP (%)	LTO	34.3±10	32.6±11.8	0.80	6	49.1±27.1	36.1±14.6	0.19	7
	SSTO	16.7±2	43.0±1.9	0.49	3	86.1±13.2	56.4±19	0.14	4
Long latency IPSP (%)	LTO	93.6±7.9	87.5±3.8	0.11	6	85.3±11.4	25.4±10.6	<0.01	7
	SSTO	83.8±3.9	81.9±11.2	0.88	3	93.5±4.7	39.9±14.4	<0.01	4
IPSP duration (ms)	LTO	512±187	518±161	0.90	6	390±26	295±14	0.02	7
	SSTO	334±179	376±138	0.38	3	219±19	198±26	0.42	4
IPSP peak amplitude (mV)	LTO	−7.6±2.0	−6.0±1.9	0.18	6	−6.5±1.5	−3.4±1.0	<0.01	7
	SSTO	−8.2±2.7	−6.7±1.3	0.37	3	−10.96±3.9	−4.2±1.8	<0.01	4
IPSP surface area (ms*mV)	LTO	2738±1806	2261±1268	0.57	6	1737±599	654±150	<0.01	7
	SSTO	1871±474	1896±458	0.27	3	1718±882	484±245	0.04	4
Rebound (%)	LTO	60.1±32	57.4±28.3	0.21	6	68.2±21.2	69±17.3	0.46	7
	SSTO	87±9.7	84.2±5.7	0.25	3	96.5±1.4	74.2±10.5	<0.05	4
Rebound amplitude (mV)	LTO	9.52±4.2	10.9±4	0.30	6	6.9±2.3	8.1±2.9	0.09	7
	SSTO	13.9±3.7	13.5±4.2	0.81	3	10.2±2.1	11.85±2.3	0.3	4

6

Table 3. Olivary subthreshold responses to CN stimulation in presence of GABA$_A$ blocker DNDS measured in Cx-36 KO mice.

| | Oscill. behavior | GABA$_A$ blocker DNDS | | | |
		Immediately after break-in	>20 minutes after break in	p- value	n
Short latency EPSP (%)	LTO	50.7±32.9	31.7±19.3	0.051	4
	SSTO	24.3±25.3	29.2±12.5	0.266	4
Long latency IPSP (%)	LTO	96.5±8	56.6±23.5	<0.05	4
	SSTO	95.8±1.3	51.8±21.8	<0.01	4
IPSP duration (ms)	LTO	488.7±123	335.1±36.3	0.07	4
	SSTO	373.0±199	298.2±121	0.191	4
IPSP peak amplitude (mV)	LTO	−8.9±4.4	−5.3±1.8	<0.05	4
	SSTO	−10.9±3	−5.5±0.6	<0.05	4
IPSP Surface area (ms*mV)	LTO	−3203.4±1775	951.5±640	<0.05	4
	SSTO	2798.1±1636.27	795.7±284.7	<0.05	4
Rebound (%)	LTO	50.7±13.6	58.3±18.2	0.16	4
	SSTO	77.2±15.1	63.8±20	<0.05	4

doi:10.1371/journal.pone.0046360.t003

CN and IO are composed by a direct inhibitory nucleo-olivary pathway and by a disynaptic excitatory loop passing through the MDJ [41]. The stimulation of the CN can activate both pathways and consequently, based on pathway length, might be expected to elicit an EPSP in olivary cells after the occurrence of the IPSP. However, this sequence was never observed in our experiments (also see Ruigrok and Voogd, [7]); when an EPSP was evoked it always preceded the IPSP. This phenomenon can be explained by the fact that somatic GABA$_A$ receptors of olivary neurons have slow activation kinetics, due to their slow-activating subunit composition ($\alpha_3\beta_{2/3}\gamma_2$, Devor et al., [25]), and that the release of neurotransmitter at the DC-IO synapse is asynchronous (Best and Regehr, [24]). This explains why the disynaptic EPSP can outpace the monosynaptic IPSP before the full-blown GABAergic shunting prevents any further electrical signaling. This hypothesis is also in line with the double stimulation experiments, which show how IO neurons undergo a long period of about 350 ms in which no excitatory input can be processed during the inhibitory phase of the response.

To confirm that the response we observed is due to direct activation of synapses that are directly connected to the recorded neuron rather then by an indirect activation through gap junctions as proposed by Ruigrok and Voogd [7], we performed a set of experiments in mice lacking the gap junction protein Connexin36. In these knock-out mice, we did not observe any difference in the sequence of the responses compared to that observed in the wild type littermates. The neuronal coupling between olivary neurons is, therefore, not required for the sequence and duration of the hyperpolarization indicating that they most likely reflect synaptic activation of the primary neuron.

Our experiments demonstrate that CN activation exerts a powerful inhibition of the IO and that all olivary neurons undergo a long-lasting silence. The hyperpolarization we observed is two times longer than that previously described in the cat by Ruigrok and Voogd [7]. This discrepancy can be attributed to either the difference in animal model, stimulation site or anesthetics. Our olivary neurons express different subthreshold profiles [22] which influence the response to CN activation. However, it's still unclear whether the LTO and SSTO neurons reflect two different populations of IO cells or simply two different

activity states of the same olivary neuron. In principle, the length of the inhibition was dependent on the state of the membrane potential. The relationship between the subthreshold profile and the length of the inhibition allow the system to influence the pattern generator (i.e. oscillations) very efficiently in a discrete temporal manner [47,48]. After the strong inhibition, SSTO neurons show an intriguing rebound depolarization that is followed by a re-initiation of the sinusoidal subthreshold oscillation as shown in Figure 2B. It is noteworthy that the chances to observe a rebound depolarization are reduced in SSTO neurons after 20 minutes of DNDS perfusion (Table 2). This is probably due to the reduced GABA$_A$-mediated hyperpolarization caused by the DNDS, which prevents the cell to generate the rebound de-polarization. When the rebound depolarization is abolished then the oscillation is not re-initiated and there is no phase-locked oscillation. In this situation the subthreshold oscillation often reappears spontaneously after a while. Overlays of many olivary responses revealed the temporal accuracy of the oscillations and the speed/time at which oscillations can shift their phase after the stimulation of the CN. The phase-lock and decay in phase-match of the oscillation, studied here at a single cell level, are proportional to the duration of the GABAergic inhibition: short IPSPs are followed by a short decay in phase-match, whereas long IPSP is followed by much slower decay process. The duration of the GABAergic inhibition (i.e. hyperpolarization and shunting) is controlling the temporal accuracy of the oscillation. Our in-terpretation is that the asynchronous release of GABA [24] determines two different features of the GABAergic response: the first is the IPSP and the second is the phase-lock of the newly generated sinusoidal oscillation. The phase lock is only temporary and fades away within the following 800 ms. Since the asynchro-nous nature of GABA release at CN to IO synapse modulates the long-lasting IPSP according to the amount of neurotransmitter released [24], we hypothesize that a longer IPSP is caused by the activation of more CN-IO fibers. A more abundant asynchronous long-lasting release of neurotransmitter, however, would not only affect the duration of the IPSP itself, but probably will also have lingering effects on subsequent oscillations, which will be reflected in the duration of the phase-lock of the sinusoidal oscillations. These two features probably underlie the two roles of the IO, the
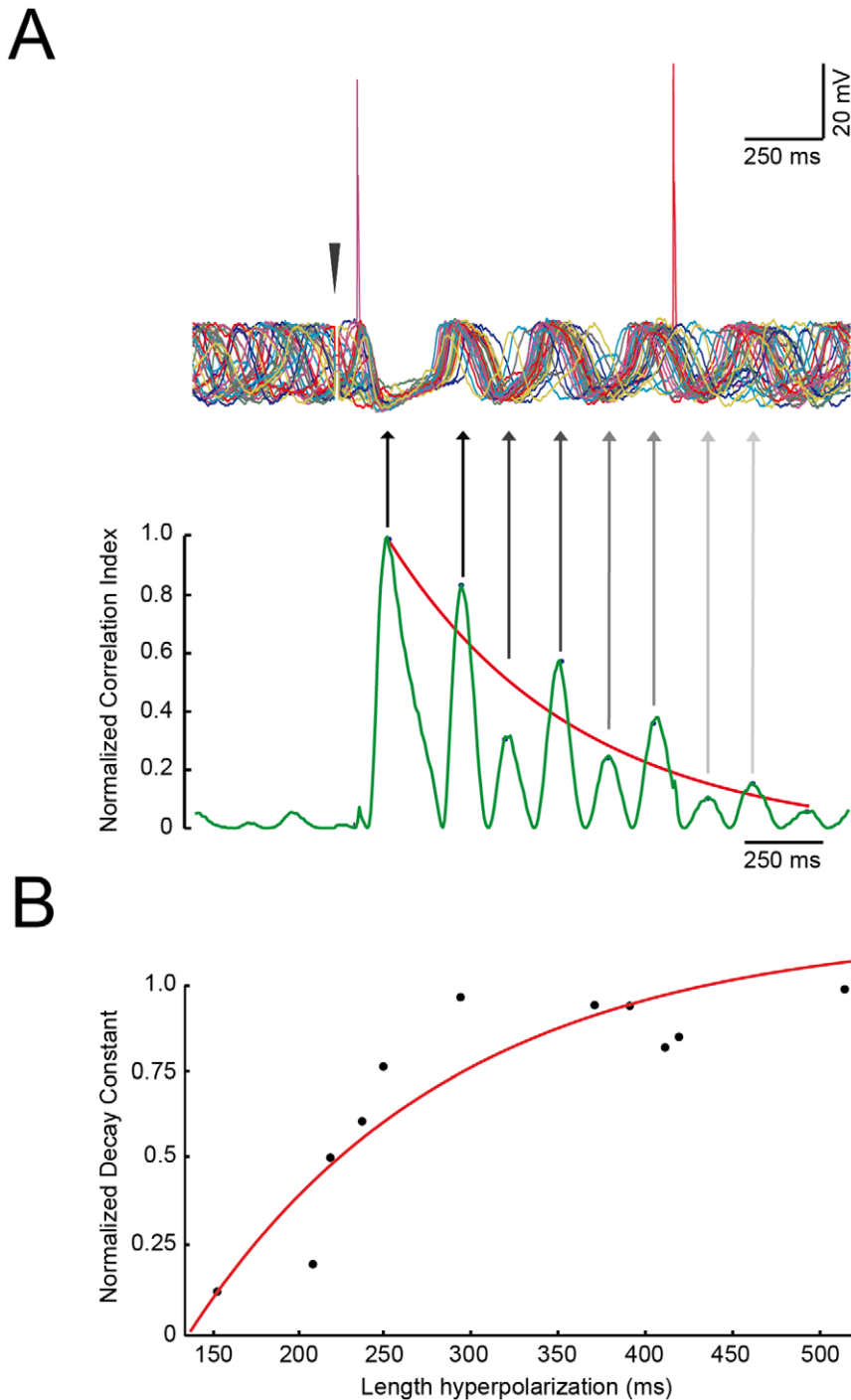
Figure 4. The length of the IPSP dictates the length of the phase reset. A, top: overlay of 36 random-start recording from the same unit, the stimulation artifact has been removed for clarity and substituted with a red arrowhead. A, bottom: cross-correlogram of the traces in A, top, normalized values are on the left bar. Arrows indicate the correspondence of the peak in the cross-correlogram with the rough recording. Blue dots indicate the points used for the exponential fitting that is shown as a red curve. C: the decay time of the exponential fittings plotted against the length of the hyperpolarization of each SSTO neuron are fitted with an exponential function (n = 11, r² = 0.83).
doi:10.1371/journal.pone.0046360.g004

former being the gating (caused by the IPSP) and the latter being the generation of temporal patterns (a longer phase-lock in the oscillations might indicate a reduced influence of the surrounding network).

Therefore, GABAergic input from the CN not only blocks temporarily all electrical signals, but it is also involved in the resetting of the temporal pattern generator (i.e. the sinusoidal subthreshold oscillation) and its temporal precision in the following cycles. Our results show for the first time how the IO is controlled by the feedback of the nucleo-olivary pathway: the activation of the CN elicits an IPSP which actively suppresses the instructive signal of the IO for approximately the length of one oscillation

cycle (i.e. gating mechanism), and simultaneously resets the phase of the oscillation itself. This feedback gating mechanism corresponds with the neuronal correlate for motor learning proposed by Andersson [2]. In their model, the CN feedback to the IO is important for blocking the teaching signal when motor learning is already optimized and for extinction of the motor task when it is not relevant anymore [10,37,49–53].

Materials and Methods

C57BL/6 male mice were imported from Harlan and housed at Erasmus MC in a 12-hour light-dark regime. Food and water were provided ad libitum. All animal procedures were in accordance with the guidelines of the Dutch Ethical Committee (DEC) at Erasmus Medical Center and the present study has been approved by the Institutional Animal Care and Use Committee (IACUC) of the Erasmus MC.

Stimulus Electrode Placement

The animals were anesthetized with a mixture of ketamine and xylazine (65 and 10 mg/kg i.p), and body temperature was maintained at 37°C with the use of an anal thermosensor and a heating pad (FHC, Bowdoinham, ME). The occipital region of the skull was cleaned and a small opening was made in the occipital bone. Extracellular pipettes filled with 3 M K-Acetate were placed in the Interpositus Nucleus of the CN using stereotaxic coordinates. Extracellular signals were amplified with a CyberAmp 380 (Axon Instruments, Foster City, CA) and spiking patterns (irregular firing pattern below 10 Hz) were used to confirm the correct location. The extracellular pipette was removed and replaced by a custom-made bipolar epoxy-insulated tungsten electrode (impedance ~300 kΩ) that was carefully lowered to the same position in the CN, either in the anterior or posterior interpositus nucleus. The recorded neurons in the olive where located in subnuclei receiving these projections, namely the caudolateral part of the Dorsal Accessory Olive (DAO) and in the rostral and central part of the Medial Accessory Olive (MAO) respectively. This is in accordance with the general topography of nucleo-olivary connections as they have been established in the rat [4]. The stimulus electrode was then glued to the occipital bone of the mouse. Misplacement of the stimulus electrode resulted in either a lack of olivary response or in a short-delayed response evoked by antidromical activation of collaterals of the climbing fibre. These fast responses were comparable with the ones previously described by Llinas and Yarom [14]: they are characterized by constant and short stimulation latency (less then 4 ms). Furthermore, the antidromic activation of the climbing fibre collaterals always elicits an action potential in olivary neurons (i.e. no failures). We exclude recordings obtained by misplaced stimulation electrodes and antidromically activated neurons. The stimulations protocol consisted of short high frequency bipolar stimulations (3 pulses; pulse frequency: 300 Hz; pulse duration: 0.2–0.3 ms; pulse intensity: <0.1 mA). Under our experimental conditions, we were not able to induce inhibitory or excitatory responses in olivary neurons by long low-frequency bipolar stimulations of the CN (3, 20 or 40 pulses; pulse frequency: 20 Hz; pulse duration: 0.2–0.3 ms; pulse intensity: <0.1 mA, as described by Best and Regher., 2009). Instead, our stimulus protocol was similar to the one described by [7] and represents the fast rebound burst spiking of CN neurons after a strong inhibition [42,54]. At the end of the experiment, a lesion was made with high-intensity current injection to confirm the position of the tungsten electrode (Figure 1C).

In Vivo Whole-Cell Recordings

To perform stable in vivo recordings in the IO, the mouse was placed in supine position and the head was restrained. In this way a ventral approach of the medulla oblongata was performed and the dura mater was removed to expose the ventral surface of the brainstem (Khosrovani et al. [22]). Whole-cell recordings were performed with borosilicate pipettes (with filament; outer diameter: 1.5 mm; inner diameter: 0.86 mm; Sutter, California, USA) filled with 4 mM NaCl, 3.48 mM MgCl$_2$, 9 mM KCl, 10 mM KOH, 120 mM K-gluconate, 10 mM Hepes, 29 mM sucrose, 4 mM Na$_2$ATP, and 0.4 mM Na$_3$GTP with pH 7.2 and osmolarity at 290–310 mOsm/kg. In the pharmacological experiments, 5 mM 4,4-dinitrostilbene-2,2′-disulfonate (DNDS; GABA$_A$ receptors blocker [29,30] was added to the pipette solutions and pH and osmolarity corrections were made. Electrode resistances ranged between 4–8 MΩ and the junction potential was approximately −8 mV; membrane potentials were corrected for this value. Current clamp recordings were amplified with a Multiclamp 700B (Axon Instruments, Foster City, CA), filtered at 10 kHz and digitized at 20 kHz with a Digidata 1322A (Axon Instruments). Membrane passive properties were determined as in Khosrovani et al. [22]; resting membrane potential of SSTO neurons refers to the mean value of the membrane potential between the peak and the trough. It has been shown that NMDA receptors are fundamental for the generation of sinusoidal oscillations [19] and for this reason the use of Ketamine/Xylazine in our experimental approach could be arguable. However, Khosrovani et al. [22] showed how the use of different anesthetics (Medetomidine-Midazolam-Fentanyl) gives result comparable to the ones observed under Ketamine/Xylazine anesthesia. Moreover, the subthreshold oscillations recorded in our experiments (both LTO and SSTO) are in line with the ones observed in vitro [14,17,26], and also in vivo using a different anesthetic, halothane [21]. In conclusion, we used Ketamine/Xylazine anesthesia because it was necessary and because, to our knowledge, it does not show any specific effect in the IO.

Data Analyses and Statistics

Data analyses were performed on neurons with resting membrane potentials negative to −45 mV and stable access and stable membrane resistances throughout the recording. Data analyses were performed with Clampfit software 9.2 (Axon Instruments, Foster City, CA).

Stimulation protocols were repeated at least 36 times for each neuron. In between the stimulation sessions the neurons' activity was monitored to discard those elements whose input resistance varied more than 20% of the initial value during the recording. In olivary neurons, excitatory postsynaptic potentials (EPSP) and inhibitory postsynaptic potentials (IPSP) were all evoked by CN stimulation. On some occasions the evoked EPSP was strong enough to elicit a sodium spike followed by afterdepolarization (ADP, as described by Llinas and Yarom [14] and Ruigrok and Voogd [7]), but in most cases only a subthreshold response was observed. The percentage of successful responses was calculated by counting the number of responses and dividing the total by the total number of stimulations. The response delay was determined by measuring the latency between the last stimulation and the start of the evoked depolarization. Of all evoked IPSPs, the peak value of the hyperpolarization and the surface area generated by the hyperpolarized membrane potential were determined. This surface area was measured between the starting point and endpoint of the IPSP by an integration algorithm implemented in Clampfit 10.2. The starting point and endpoint of IPSPs were determined by using a threshold potential of −2 mV negative to

the resting membrane potential. If there was any subthreshold sinusoidal oscillation the resting membrane potential (Vm) was determined from the (low-pass) readout of the baseline potential. The rebound depolarization at the end of the long latency IPSP was identified as an upward deflection of the membrane potential that was at least 2 mV greater than the value of the membrane potential preceding the IPSP. In order to investigate the impact of the subthreshold oscillation on the CN induced response, we subdivided the olivary cells into two groups on the basis of their subthreshold activity: the spontaneous 3 – to 12 Hz sinusoidal subthreshold oscillating cells (SSTO) and the spontaneous 1 – to 3 Hz low-threshold Ca^{2+} oscillating cells (LTO). The use of the frequencies of subthreshold oscillations to categorize different groups of olivary cell has been justified by cluster analysis in Khosrovani et al. [22]. Comparison between groups and conditions were made by using two-tailed Student's t-test, and p values were adjusted by using the Bonferroni correction method. All the values express average ± standard deviation (SD). Cross-correlograms were performed in the Matlab (The MathWorks, Inc., Natick, MA) environment using a custom-made function. The aim of the analysis was to measure the kinetics of the CN-activation induced phase-lock and the developing phase variance of the sinusoidal subthreshold oscillations. For each recorded SSTO neuron, 36 randomly-started stimulations were analyzed, and cross-correlograms were computed between all the possible combinations of couples of stimulations (i.e., 36*36 = 1296 combinations) using a "running window" of 100 ms that shifted along the full length of the recordings by 50 ms steps. The cross-correlograms computed between all the possible combinations of pairs of recordings were then averaged and fitted with a single exponential function to extract the time constant from all of the 11 SSTO neurons analyzed (Figure 4). The decay time constants of the cross correlograms were plotted against the length of the

hyperpolarization, and this data set was fitted using a single exponential function.

Supporting Information

Figure S1 Double stimulation experiments. An LTO neuron responding with a short latency EPSP is stimulated twice at different time intervals (first trace single stimulation, then 25, 175, 250, 350 ms intervals respectively, stimulation artifacts are indicated by red arrow heads). A second EPSP is evoked when the time interval is at least 350 ms (indicated by the asterisk). Every trace represents the average of 12 repetitions.
(TIF)

Figure S2 Experiment performed with 15mM DNDS. Wild type SSTO cell (top trace) responding to CN stimulation, then (middle trace) the response of the same cell to CN stimulation in reduced after 20 minutes of dialysis with DNDS 15 mM, bottom trace represents the averages at the beginning of the experiment (black) and after 20 minutes of DNDS 15 mM (red). Even with high concentration of DNDS the IPSP is not completely abolished.
(TIF)

Author Contributions

Conceived and designed the experiments: PB TR CDZ MDJ. Performed the experiments: PB. Analyzed the data: PB MDJ. Contributed reagents/materials/analysis tools: PS. Wrote the paper: PB TR CDZ MDJ.

References

1. Llinas R, Baker R, Sotelo C (1974) Electrotonic coupling between neurons in cat inferior olive. J Neurophysiol 37: 560–571.
2. Andersson G, Garwicz M, Hesslow G (1988) Evidence for a GABA-mediated cerebellar inhibition of the inferior olive in the cat. Exp Brain Res 72: 450–456.
3. Hesslow G (1986) Inhibition of inferior olivary transmission by mesencephalic stimulation in the cat. Neurosci Lett 63: 76–80.
4. Ruigrok TJ, Voogd J (1990) Cerebellar nucleo-olivary projections in the rat: an anterograde tracing study with Phaseolus vulgaris-leucoagglutinin (PHA-L). J Comp Neurol 298: 315–333.
5. Angaut P, Sotelo C (1989) Synaptology of the cerebello-olivary pathway. Double labelling with anterograde axonal tracing and GABA immunocytochemistry in the rat. Brain Res 479: 361–365.
6. Fredette BJ, Mugnaini E (1991) The GABAergic cerebello-olivary projection in the rat. Anat Embryol 184: 225–243.
7. Ruigrok TJ, Voogd J (1995) Cerebellar influence on olivary excitability in the cat. Eur J Neurosci 7: 679–693.
8. De Zeeuw CI, Holstege JC, Ruigrok TJ, Voogd J (1990) Mesodiencephalic and cerebellar terminals terminate upon the same dendritic spines in the glomeruli of the cat and rat inferior olive: an ultrastructural study using a combination of [3H]leucine and wheat germ agglutinin coupled horseradish peroxidase anterograde tracing. Neuroscience 34: 645–655.
9. Ruigrok TJ (2010) Ins and Outs of Cerebellar Modules. Cerebellum: In press.
10. Medina JF, Nores WL, Mauk MD (2002) Inhibition of climbing fibres is a signal for the extinction of conditioned eyelid responses. Nature 416: 330–333.
11. Llinas RR (2011) Cerebellar motor learning versus cerebellar motor timing: the climbing fibre story. J Physiol 589: 3423–3432.
12. Bengtsson F, Svensson P, Hesslow G (2004) Feedback control of Purkinje cell activity by the cerebello-olivary pathway. Eur J Neurosci 20: 2999–3005.
13. Lang EJ, Sugihara I, Llinas R (1996) GABAergic modulation of complex spike activity by the cerebellar nucleoolivary pathway in rat. J Neurophysiol 76: 225–275.
14. Llinas R, Yarom Y (1986) Oscillatory properties of guinea-pig inferior olivary neurones and their pharmacological modulation: an in vitro study. J Physiol 376: 163–182.
15. Sotelo C, Gotow T, Wassef M (1986) Localization of glutamic-acid-decarboxylase-immunoreactive axon terminals in the inferior olive of the rat,

with special emphasis on anatomical relations between GABAergic synapses and dendrodendritic gap junctions. J Comp Neurol 252: 32–50.
16. De Zeeuw CI, Holstege JC, Ruigrok TJ, Voogd J (1989) Ultrastructural study of the GABAergic, cerebellar, and mesodiencephalic innervation of the cat medial accessory olive: anterograde tracing combined with immunocytochemistry. J Comp Neurol 284: 12–35.
17. Bal T, McCormick DA (1997) Synchronized oscillations in the inferior olive are controlled by the hyperpolarization-activated cation current I(h). J Neurophysiol 77: 3145–3156.
18. Llinas R, Yarom Y (1981) Electrophysiology of mammalian inferior olivary neurones in vitro. Different types of voltage-dependent ionic conductances. J Physiol 315: 549–567.
19. Placantonakis D, Welsh J (2001) Two distinct oscillatory states determined by the NMDA receptor in rat inferior olive. J Physiol 534: 123–140.
20. Devor A, Yarom Y (2000) GABAergic modulation of olivary oscillations. Prog Brain Res 124: 213–220.
21. Chorev E, Yarom Y, Lampl I (2007) Rhythmic episodes of subthreshold membrane potential oscillations in the rat inferior olive nuclei in vivo. J Neurosci 27: 5043–5052.
22. Khosrovani S, Van Der Giessen RS, De Zeeuw CI, De Jeu MT (2007) In vivo mouse inferior olive neurons exhibit heterogeneous subthreshold oscillations and spiking patterns. Proc Natl Acad Sci U S A 104: 15911–15916.
23. Van Der Giessen RS, Koekkoek SK, van Dorp S, De Gruijl JR, Cupido A, et al. (2008) Role of olivary electrical coupling in cerebellar motor learning. Neuron 58: 599–612.
24. Best AR, Regehr WG (2009) Inhibitory regulation of electrically coupled neurons in the inferior olive is mediated by asynchronous release of GABA. Neuron 62: 555–565.
25. Devor A, Fritschy JM, Yarom Y (2001) Spatial distribution and subunit composition of GABA(A) receptors in the inferior olivary nucleus. J Neurophysiol 85: 1686–1696.
26. Long MA, Deans MR, Paul DL, Connors BW (2002) Rhythmicity without synchrony in the electrically uncoupled inferior olive. J Neurosci 22: 10898–10905.
27. De Zeeuw CI, Chorev E, Devor A, Manor Y, Van Der Giessen RS, et al. (2003) Deformation of network connectivity in the inferior olive of connexin 36-

deficient mice is compensated by morphological and electrophysiological changes at the single neuron level. J Neurosci 23: 4700–4711.

28. Leznik E, Llinas R (2005) Role of gap junctions in synchronized neuronal oscillations in the inferior olive. J Neurophysiol 94: 2447–2456.

29. Bridges RJ, Worrell RT, Frizzell RA, Benos DJ (1989) Stilbene disulfonate blockade of colonic secretory Cl- channels in planar lipid bilayers. Am J Physiol 256: C902–912.

30. Dudek SM, Friedlander MJ (1996) Intracellular blockade of inhibitory synaptic responses in visual cortical layer IV neurons. J Neurophysiol 75: 2167–2173.

31. Turgeon SM, Albin RL (1994) GABAB binding sites in early adult and aging rat brain. Neurobiol Aging 15: 705–711.

32. Turgeon SM, Albin RL (1994) Postnatal ontogeny of GABAB binding in rat brain. Neuroscience 62: 601–613.

33. Sotelo C, Llinas R, Baker R (1974) Structural study of inferior olivary nucleus of the cat: morphological correlates of electrotonic coupling. J Neurophysiol 37: 541–559.

34. Yarom Y, Llinas R (1987) Long-term modifiability of anomalous and delayed rectification in guinea pig inferior olivary neurons. J Neurosci 7: 1166–1177.

35. Choi S, Yu E, Kim D, Urbano FJ, Makarenko V, et al. (2010) Subthreshold membrane potential oscillations in inferior olive neurons are dynamically regulated by P/Q- and T-type calcium channels: a study in mutant mice. J Physiol 588: 3031–3043.

36. Park YG, Park HY, Lee CJ, Choi S, Jo S, et al. (2010) Ca(V)3.1 is a tremor rhythm pacemaker in the inferior olive. Proc Natl Acad Sci U S A 107: 10731–10736.

37. Bengtsson F, Hesslow G (2006) Cerebellar control of the inferior olive. Cerebellum 5: 7–14.

38. Svensson P, Bengtsson F, Hesslow G (2006) Cerebellar inhibition of inferior olivary transmission in the decerebrate ferret. Exp Brain Res 168: 241–253.

39. De Zeeuw CI, Ruigrok TJ, Holstege JC, Jansen HG, Voogd J (1990) Intracellular labeling of neurons in the medial accessory olive of the cat: II. Ultrastructure of dendritic spines and their GABAergic innervation. J Comp Neurol 300: 478–494.

40. De Zeeuw CI, Ruigrok TJ, Holstege JC, Schalekamp MP, Voogd J (1990) Intracellular labeling of neurons in the medial accessory olive of the cat: III. Ultrastructure of axon hillock and initial segment and their GABAergic innervation. J Comp Neurol 300: 495–510.

41. De Zeeuw CI, Ruigrok TJH, Hawkins R, van Alphen AM (1997) Climbing fiber collaterals contact neurons in the cerebellar nuclei that provide a GABAergic feedback to the inferior olive.

42. Hoebeek FE, Witter L, Ruigrok TJ, De Zeeuw CI (2010) Differential olivo-cerebellar cortical control of rebound activity in the cerebellar nuclei. Proc Natl Acad Sci U S A 107: 8410–8415.

43. Gruart A, Blazquez P, Pastor AM, Delgado-Garcia JM (1994) Very short-term potentiation of climbing fiber effects on deep cerebellar nuclei neurons by conditioning stimulation of mossy fiber afferents. Exp Brain Res 101: 173–177.

44. Sanchez-Campusano R, Gruart A, Delgado-Garcia JM (2009) Dynamic associations in the cerebellar-motoneuron network during motor learning. J Neurosci 29: 10750–10763.

45. De Zeeuw CI, Hoebeek FE, Bosman LW, Schonewille M, Witter L, et al. (2011) Spatiotemporal firing patterns in the cerebellum. Nat Rev Neurosci 12: 327–344.

46. Person AL, Raman IM (2011) Purkinje neuron synchrony elicits time-locked spiking in the cerebellar nuclei. Nature 481: 502–505.

47. Kistler WM, De Zeeuw CI (2002) Dynamical working memory and timed responses: the role of reverberating loops in the olivo-cerebellar system. Neural Comput 14: 2597–2626.

48. Kistler WM, De Jeu MT, Elgersma Y, Van Der Giessen RS, Hensbroek R, et al. (2002) Analysis of Cx36 knockout does not support tenet that olivary gap junctions are required for complex spike synchronization and normal motor performance. Ann N Y Acad Sci 978: 391–404.

49. Hesslow G, Ivarsson M (1996) Inhibition of the inferior olive during conditioned responses in the decerebrate ferret. Exp Brain Res 110: 36–46.

50. Kim JH, Wang JJ, Ebner TJ (1988) Alterations in simple spike activity and locomotor behavior associated with climbing fiber input to Purkinje cells in a decerebrate walking cat. Neuroscience 25: 475–489.

51. Medina JF, Garcia KS, Mauk MD (2001) A mechanism for savings in the cerebellum. J Neurosci 21: 4081–4089.

52. Sears LL, Steinmetz JE (1991) Dorsal accessory inferior olive activity diminishes during acquisition of the rabbit classically conditioned eyelid response. Brain Res 545: 114–122.

53. McCormick DA, Steinmetz JE, Thompson RF (1985) Lesions of the inferior olivary complex cause extinction of the classically conditioned eyeblink response. Brain Res 359: 120–130.

54. Sangrey T, Jaeger D (2010) Analysis of distinct short and prolonged components in rebound spiking of deep cerebellar nucleus neurons. Eur J Neurosci 32: 1646–1657.